Some physical parameters of CuInGaS$_2$ thin films deposited by spray pyrolysis for solar cells

Ahmed Kotbi[1,2] · Bouchaib Hartiti[1] · Salah Fadili[1] · Abderraouf Ridah[2] ·
Philippe Thevenin[3]

Abstract Copper–indium–gallium–disulphide (CuInGaS$_2$) is a promising absorber material for thin film photovoltaic. In this paper, CuInGaS$_2$ (CIGS) thin films have been prepared by chemical spray pyrolysis method onto glass substrates at ambient atmosphere. Structural, morphological, optical and electrical properties of CuInGaS$_2$ films were analysed by X-ray diffraction (XRD), Raman spectroscopy, scanning electron microscopy (SEM), UV–Vis spectrophotometer and Hall Effect measurement, respectively. The films exhibited single phase chalcopyrite structure. The strain and dislocation density decreased with increase of spray time. The grain size of the films increased from 4.45 to 9.01 nm with increase of spray time. The Raman spectrum indicated the presence of the principal chalcopyrite peak at 295 cm^{-1}. The optical properties of the synthesized films have been carried out through the measurement of the absorbance spectrum. The optical band gap was estimated by the absorption spectrum fitting (ASF) method. For each sample, the width of the band tail (E_{Tail}) of CuInGaS$_2$ thin films was determined. The resistivity (ρ), conductivity (σ), mobility (μ), carrier concentration and conduction type of the films were determined using Hall Effect measurements. The interesting optical properties of CuInGaS$_2$ make them an attractive material for photovoltaic devices.

✉ Ahmed Kotbi
   kotbi.ahmed7@gmail.com

1   MAC&PM Laboratory, ANEPMAER Group, FSTM, Hassan II Casablanca University, B.P 146, Mohammedia, Morocco

2   LIMAT Laboratory, Department of Physics, FSB, Hassan II Casablanca University, B.P 7955, Casablanca, Morocco

3   LMOPS Laboratory, Department of Physics, University of Lorraine, Metz, France

1 Introduction

Copper–Indium–Gallium–Sulfide (CIGS) quaternary film with chalcopyrite structure is a promising absorber material for photovoltaic applications and solar cells. This is mainly due to its direct band gap of about 1.50 eV and a high optical absorption coefficient of $\sim 10^5$ cm^{-1} in the visible spectral range [1]. Many methods, such as sputtering [2], co-evaporation [3], chemical spray pyrolysis (CSP) [4, 5], and electrodeposition [6], have been developed for the deposition of CIGS films. We have been using a chemical spray pyrolysis system for deposition CuInGaS$_2$ thin films. This method does not require vacuum and films may be deposited on a large area. The composition of the films can be controlled easily by varying the concentration of components in the spray solution. Therefore, films with various compositions can be prepared unlike all other deposition processes. The ease with which the doping can be done by incorporating the dopants in a spray solution and the possibility of varying stoichiometry of samples by varying the atomic ratio of the spray solutions of the components are the other advantages of this technique [7].

In the present work, the fabricated films were characterized by using X-ray diffraction (XRD), Raman spectroscopy, scanning electron microscopy (SEM), UV–Vis spectrophotometer and Hall Effect measurement. XRD data used to calculate the grain size, dislocation density and lattice strain of the spray pyrolyzed CuInGaS$_2$ thin films. The morphological property is studied using scanning electron microscopy (SEM). We use the absorption spectra fitting procedure (ASF) to obtain the band gap of CuInGaS$_2$ thin films semiconductors that only requires the measurement of the absorbance spectra and without the need of additional information, such as the film thickness or

reflectance spectra [8, 9]. For each sample, the width of the band tail of the CuInGaS$_2$ was determined. Based on these measurement results, we will discuss the growth properties of CuInGaS$_2$ films. So, we have two purposes in this work; the first is determining of the optical band gap and tailing states and the second is to discuss about some of the structural, morphological and electrical properties of CuInGaS$_2$ thin films.

2 Experimental details

The CuInGaS$_2$ thin films were deposited by spray pyrolysis method on ordinary glass slices. Prior to deposition, the glass substrates were chemically cleaned with acetone, ethanol and double distilled water separately. The copper (II) chloride, indium (III) chloride and thiourea are mixed to form CuInS$_2$ material. The following reaction gives the reasonable mechanism responsible for the formation of CuInS$_2$ thin films [10]:

$$CuCl + InCl_3 + 2SC(NH_2)_2 + 4H_2O$$
$$\Rightarrow CuInS_2 + 2CO_2 + 4NH_4Cl \tag{1}$$
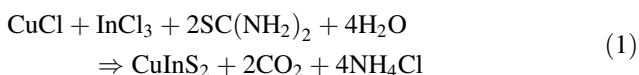
The gallium (III) chloride was added to the starting solution to obtain CuInGaS$_2$ thin films. During the deposition process, the precursor solution is pulverized onto the substrates using compressed air as carrier gas. CuInGaS$_2$ thin films with Cu:In ratio 1.1, Ga:In ratio 0.05 and S:Cu ratio 3.63 were prepared using different times of spray 25, 30 and 40 min, keeping all other parameters constant. The distance between spray head and substrate was maintained at 30 cm. Substrate temperature was kept constant at 375 °C during all experiments, because this temperature is found in our previous work as the optimum temperature that gives better optical and electrical properties of CuInS$_2$ thin films [11]. The spray rate was 1.6 ml/min. Spray pyrolysis is responsible for the formation of a fine vapor of very small droplets containing the reactants onto the hot substrates. At substrate temperature of 375 °C, the solvent (double distilled water) evaporates before the droplet arrives the substrate. Then the CuInGaS$_2$ precipitate melts and vaporizes in air without decomposition. Finally, the vapor diffuses on the glass substrate to undergo thermal decomposition process, which then result into the film formation [12]. The crystallographic structure was studied by a instead an X-ray diffractometer (XRD) with CuKα radiation ($\lambda = 0.154$ nm) at 2θ from 20° to 75°. Williamson–Hall method was used for estimating average grain size and effective lattice strain. The crystal structure of the films was confirmed using Raman spectra. The surface morphology is studied using scanning electron microscopy (SEM). The spectral absorbance of the films

was recorded in the wavelength range 500-900 nm by using a UV–Vis spectrophotometer and the electrical properties [the resistivity (ρ), conductivity (σ), mobility (μ), carrier concentration and type of conductivity] of the films were measured by Hall Effect measurement.

3 Result and discussions

3.1 Structural properties

Figure 1 shows the X-ray diffraction pattern of the CuInGaS$_2$ thin films with various spray times. All of the samples are consistent with the chalcopyrite (tetragonal) crystal structure in the anticipated 2θ position for the (112), (220/204) and (312/116) crystal planes (ICDD card No: 00-027-0159) [13]. No other phases were observed in the X-ray diffractograms indicating the formation of single phase material. All samples were polycrystalline in nature. The intensity of (112) peak corresponding to CuInGaS$_2$ increased with spray time.

Microstructural parameters were estimated by studying the X-ray diffractograms of CuInGaS$_2$ films. The tetragonal lattice parameters were calculated from the 2θ values of all hkl planes and from relations (2) and (3) [14]:

$$\frac{1}{d_{hkl}^2} = \frac{h^2 + k^2}{a^2} + \frac{l^2}{c^2} \tag{2}$$

$$n\lambda = 2d_{hkl}\sin\theta \tag{3}$$

where a and c are the lattice parameters and d_{hkl} is the lattice spacing of hkl. h, k and l are the Miller indices, λ is the wavelength of the CuK$_\alpha$ radiation (0.154 nm) and 2θ is the diffraction angle of the corresponding plane. Lattice constants were calculated to be: $a = 5.51$ Å and $c = 11.22$ Å.
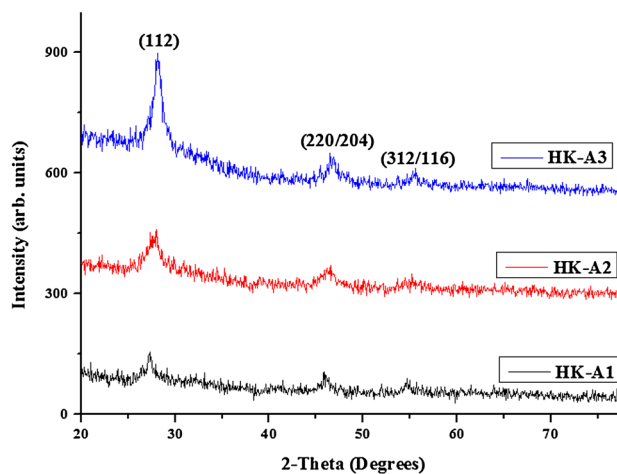

Fig. 1 XRD patterns of CuInGaS$_2$ films deposited at different times of spray

Among the available methods, Williamson–Hall analysis is a simplified method where both size and strain induced broadening is deconvoluted by considering the peak width as a function of 2θ [15]. Williamson–Hall method was used for estimating average grain size and effective lattice strain. The lattice strain (ε) defines the crystal imperfections and deformations produced in the CuInGaS$_2$ thin film. The FWHM can be expressed as a linear combination of the contributions from the lattice strain and grain size as [16, 17]:

$$\beta\cos\theta = \frac{K\lambda}{D} + 4\varepsilon\sin\theta \tag{4}$$

where K is a constant whose value was taken as 0.94, λ is the wavelength of X-ray used, β is the full-width half-maximum (FWHM), θ is the Bragg angle, D is grain size and ε is the effective lattice strain. The grain size can be estimated from the linear fit. The inverse of the y-intercept on the $\beta\cos\theta/\lambda$ axis gives a mean value of the grain size. The slope of the fitted line indicates the presence of effective strain in the crystal lattice of the CIGS thin films. The grain size varied from 4.45 to 9.01 nm as the spray time increased. Calculation of grain size from X-ray diffractograms showed that even the best crystalline films (HK-A3) had a grain size of only ~ 9 nm. Larger grain is very desirable for the fabrication of high efficient CuInS$_2$ solar cells [18]. The dislocation density δ, defined as the length of dislocation lines per unit volume of the crystal has been evaluated using the formula [19]:

$$\delta = 1/D^2 \tag{5}$$

The microstructural parameters are presented in Table 1. From the table it is observed that the dislocation density decreases with increase of grain size.

The Raman spectroscopy was used to obtain further insight into the phase identification. Confirmation of the chalcopyrite structure was underpinned by Raman spectroscopy (Fig. 2). All spectra are dominated by the A^1_{LO} mode at 295 cm^{-1}, which is the main vibrational band of the CuInS$_2$ chalcopyrite phase, corresponding to the totally symmetric vibration of the anion sublattice [20]. Figure 2 shows two other main vibrational modes identified as follows: peaks E^3_{TO} (240 cm^{-1}) and E^1_{LO} (340 cm^{-1}) are assigned to the chalcopyrite crystalline phase [21].
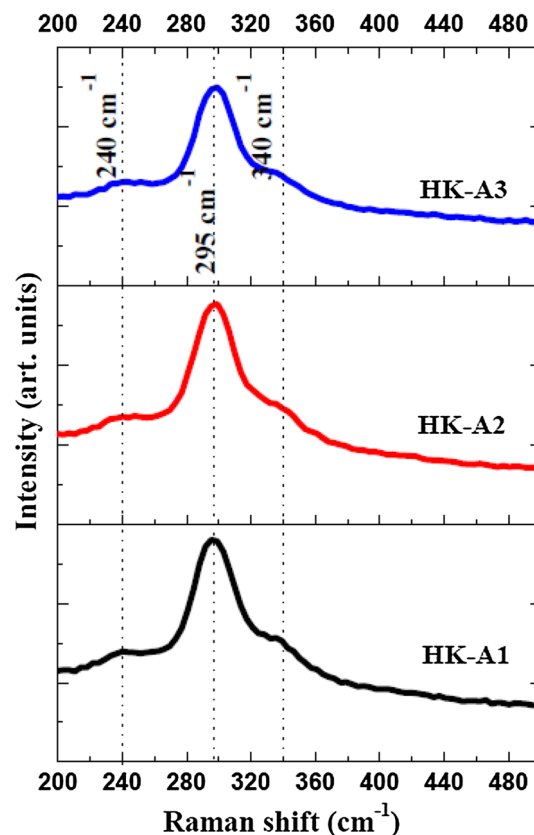

Fig. 2 Raman scattering measurements of CuInGaS$_2$ sprayed films

3.2 Morphological characterization

The surface morphologies of the films were observed by scanning electron microscopy (SEM). The SEM surface images of CuInGaS$_2$ thin films deposited at different spray times are depicted in Fig. 3. As presented, enormous morphological differences were found among CuInGaS$_2$ thin films. The film sprayed at 25 minutes shows the non continuous structure and some cavities or vacuums. For a spray time of 30 minutes, the SEM image has more apparent grains. As the spray time increases up to 40 minutes, the film surface becomes more compact with large dense grains. This type of dense and compact morphology is essential for the applications in thin film solar cells [22]. Consequently, we conclude that the surface morphologies of the thin films clearly change with the increase of the spray time.

Table 1 Some structural properties of CuInGaS$_2$ thin films

Sample name	Time of spray (min)	Grain size (nm)	δ ($\times 10^{10}$ lines mm^{-2})	Lattice strain (ε)
HK-A1	25	4.45	5.049	0.0344
HK-A2	30	7.59	1.735	0.0199
HK-A3	40	9.01	1.231	0.0166

HK-A1 (25 min)

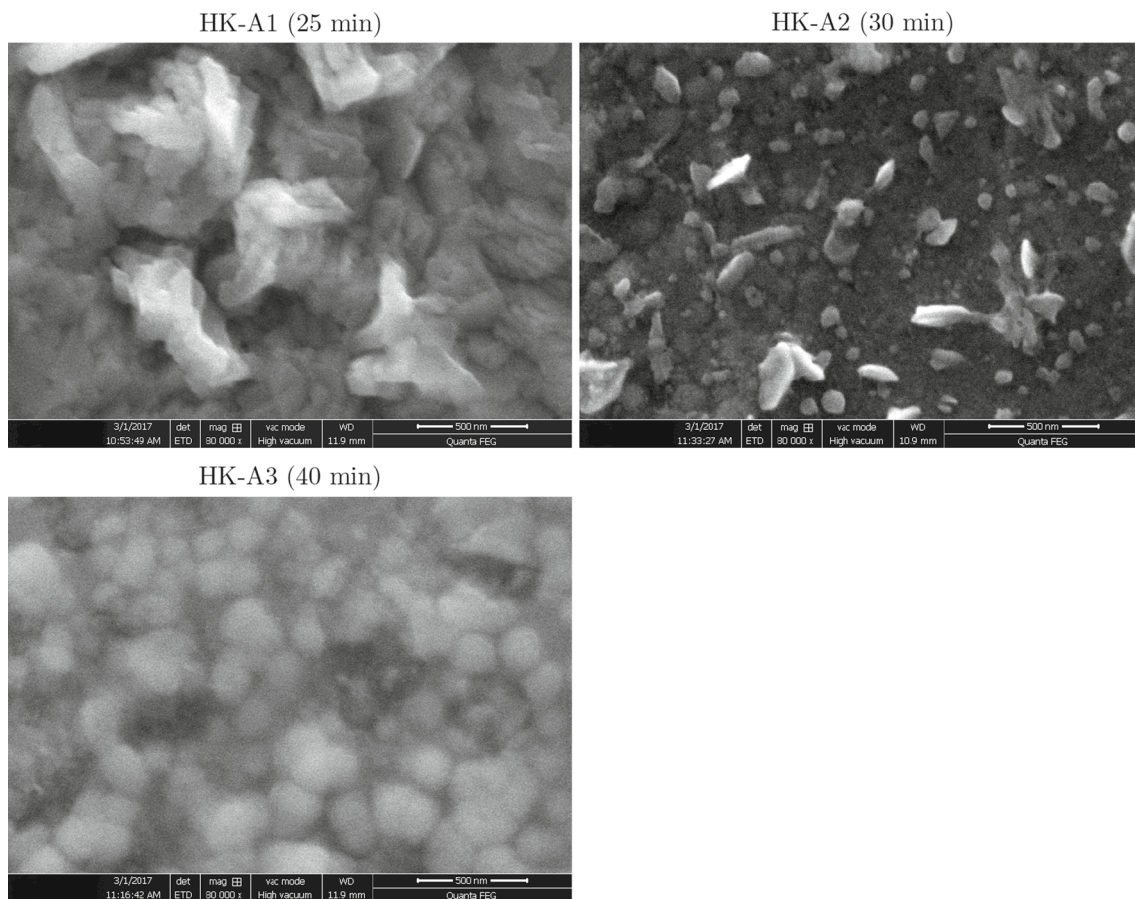HK-A2 (30 min)

HK-A3 (40 min)

Fig. 3 SEM micrographs of CuInGaS$_2$ films

3.3 Optical properties

3.3.1 Absorption spectra fitting procedure (ASF)

The absorption spectra fitting method was employed to estimate the optical band gap (E_g). It is possible to determine the energy band gap in semiconductors that only requires the measurement of the absorbance spectrum without any information on film thickness or reflectance spectra [23, 24]. This can be done by the method so-called absorption spectrum fitting (ASF) [25]. The most usual method of the band gap determination is based on measurement of the optical absorption coefficient and using the Tauc method; this method has been extensively used for different binary and ternary semiconductor films [26–29]. The energy band gap (E_g) is an important property for solar cell and photoelectrochemical device applications. To introduce the absorption spectrum fitting method, one can start with the Tauc relation for an allowed direct band gap transition (at the high optical absorption region $\alpha(\lambda) \geq 10^4 \text{cm}^{-1}$) [30–33]:

$$\alpha h v = B(h v - E_{\text{g}})^{1/2} \tag{6}$$

$h v$ refers to the photon energy, B is a constant and E_g corresponds to the direct band gap. $\alpha(\lambda)$ is the absorption coefficient defined by the Beer-Lambert's law as [34]:

$$\alpha(\lambda) = [2.303 \times Abs(\lambda)]/d \tag{7}$$

where d is the film thickness and $Abs(\lambda)$ is absorbance of the film. Fig. 4 shows the optical absorbance $Abs(\lambda)$ spectra of CuInGaS$_2$ films in the wavelength range 500–900 nm. Using the Eqs. (6) and (7), it is possible to write a new equation as a function of wavelength:

$$Abs(\lambda) = A_1 \lambda \left(\frac{1}{\lambda} - \frac{1}{\lambda_g} \right)^{1/2} + A_2 \tag{8}$$

where $A_1 = [B(hc)^{-\frac{1}{2}} \times d/2.303]$ and A_2 is a constant that reflect reflection. Employing equation (8), one can determine the optical band gap by an absorbance spectrum fitting method (ASF) without the need of the film thickness. The value of band gap can be calculated from the parameter λ_g using:
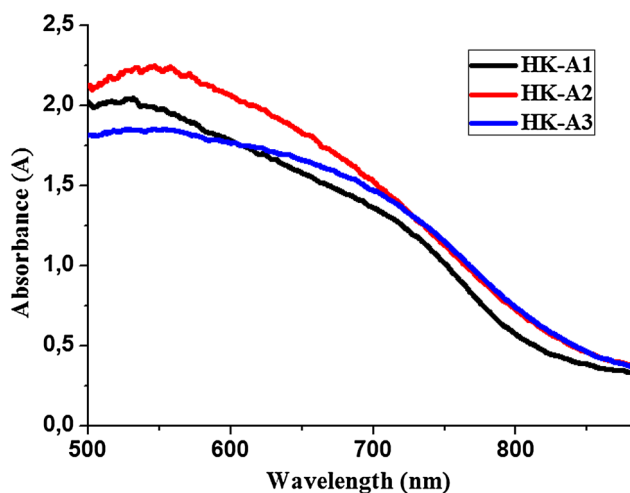
Fig. 4 Optical absorption spectra of CuInGaS$_2$ films at different deposition times
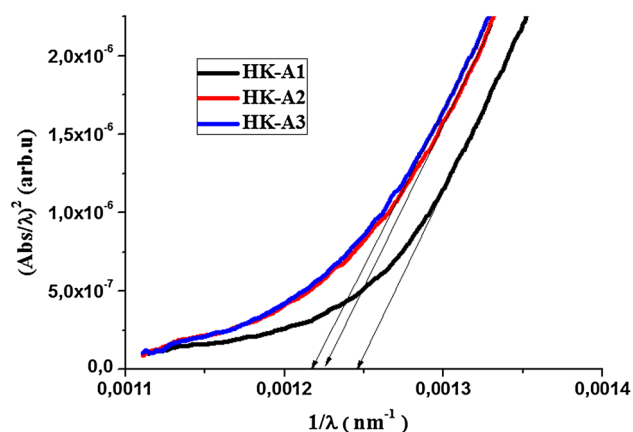

Fig. 5 Absorption spectra fitting plots for samples with 25, 30 and 40 min deposition times

$$E_{gap}^{ASF} = \frac{1239.83}{\lambda_g} \qquad (9)$$

The direct band gap is obtained by the intercept point of the ($1/\lambda$) axis by extrapolating the linear portion of $(Abs/\lambda)^2$ versus $1/\lambda$ (Fig. 5). This method can be used when there is a difficulty to measure the thickness of the films.

We can see from Table 2 that the value of band gap decreases from 1.54 eV (HK-A1) to 1.50 eV (HK-A3) following the increase of spray time. The optical analysis using the absorbance measurements Abs(λ) allow us to determine the direct band gap energy value and it is in the range 1.50–1.54 eV, which is close to the optimal theoretical value ($E_g = 1.5$ eV) [35]. This result indicates that CuInGaS$_2$ compound has an absorbing property favorable for applications in solar cell devices.

Table 2 Energy band gap and width of band tail for CuInGaS$_2$

Sample name	Time of spray (min)	E_g (eV)	E_{Tail} (eV)	R^2
HK-A1	25	1.54	0.173	0.9872
HK-A2	30	1.52	0.202	0.9889
HK-A3	40	1.50	0.205	0.9865

3.3.2 Width of the tail of localized states

In the curve of the absorption coefficient and near the optical band edge, there is an exponential part called Urbach tail. This exponential tail appears in the low crystallinity materials, poor crystallinity, disordered and amorphous materials. In the low absorption region, $\alpha(\lambda) < 10^4$ cm^{-1}, the spectral reliance of the absorption coefficient (α) and the energy of photons ($hv = hc/\lambda$) is known as Urbach empirical rule, which is given by the following equation [36, 37]:

$$\alpha(\lambda) = \alpha_0 exp\left(\frac{hc}{\lambda E_{Tail}}\right) \qquad (10)$$

where α_0 is a constant and E_{Tail} denotes the energy of the band tail or sometimes called Urbach energy, which is weakly dependent upon temperature and is often interpreted as the width of the band tail due to localized states in the normally band gap that is associated with the disordered or low crystalline materials [38]. Also, E_{Tail} is width of the tail of localized states corresponding to the optical transition between localized tail states in adjacent of valence band and extended state in the conduction band lying above the mobility edge. In absorption spectra fitting procedure, Eq. (10) can be written as:

$$Abs(\lambda) = A_3 exp\left(\frac{hc}{\lambda E_{Tail}}\right) \qquad (11)$$

where A_3 is ($\alpha_0 d/2.303$). Therefore, the band tail energy (E_{Tail}) or Urbach energy can be obtained from the slope of the straight line of plotting Ln(Abs) against the inverse of the wavelength ($1/\lambda$) (Fig. 6) using the equation:

$$E_{Tail} = \frac{1239.83}{slope} \qquad (12)$$

The least squares method was employed to calculate the E_{Tail} values. Results of these calculations have been presented in Table (2) with the coefficient of determination (R^2) is a measure of the quality of the prediction of a linear regression. It is observed that, the width of the band tail is increased by increasing of the deposition time. The behavior of (E_{Tail}) can be attributed to the increasing of the spray time, which leads to increase the disordered atoms
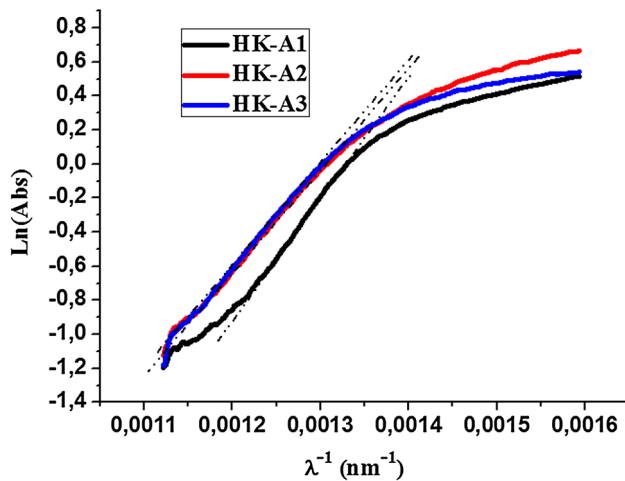
Fig. 6 Plots of Ln(Abs) vs. $(1/\lambda)$ for samples with 25,30 and 40 min deposition times

and defects in the structural bonding. The disorder and defects can introduce localized states at or near the conduction band level, which leads to increase the band tail width E_{Tail} [39, 40].

3.4 Electrical properties

In order to investigate the electrical behavior of the samples, the carrier concentration, mobility, resistivity, conductivity and conduction type of samples were determined using Hall Effect measurements. They are listed as shown in Table 3. All samples were p-type semiconductors. The positive sign of hall coefficient confirmed the p-type of conductivity for all films. Generally, the conduction type of I–III–VI$_2$ samples can be adjusted with small deviations from stoichiometry in the crystal [41, 42]. The compositional deviations from the ideal chemical formula for CuInGaS$_2$ material can be conveniently described by nonstoichiometry ($\triangle y = [(2S/(Cu+3(In+Ga)))-1])$ [43]. The $\triangle y$ parameter is related to the electronic defects and would determine the type of the majority charge carriers. Films with $\triangle y > 0$ would behave as p-type material while $\triangle y < 0$ would show n type conductivity [44]. The main donors in n-type semiconductors may be the group III atoms (In) occupying the site of group I atoms (Cu) or S vacancies. The main acceptors in p-type semiconductors may be the group I atoms (Cu) occupying the site of group III atoms (In) or S interstitials [45, 46]. The value of $\triangle y =$

$[(2S/(Cu+3(In+Ga)))-1]$ molar ratio in samples is 0.75, making them p-type semiconductors. Our study shows that CuInGaS$_2$ thin films deposited at 40 min has a good performance, compared with the others, with the carrier concentration of 7.74×10^{18} cm^{-3}, the mobility of 1.51 cm^2/$V.s$, the conductivity of 1.87 $\Omega^{-1}.$cm^{-1} and the resistivity 5.33×10^{-1} Ωcm. The high value of carrier concentration of CuInGaS$_2$ thin film is not favored for the absorber of thin film solar cells. This is due to the elimination of some defects in the samples. The previous literature survey showed that the carrier concentration of CIGS and CIS thin films with high efficiency was $\sim 10^{16}$cm^{-3} [47, 48]. Therefore, the films prepared at 25 min are not favored for solar cells despite the low resistance and high mobility. The conductivity is improved for the films deposited at 40 min and this behavior may be due to a combination of three mechanisms, namely, (i) due to diffusion of phonons and point defects, etc., (ii) from film surface and (iii) due to grain boundaries in polycrystalline films [49]. The grain boundary is defined as region between two grains. It is concluded that the conductivity of the polycrystalline films is highly dependent on the grain size. The growth in grains leads to a reduction in the diffusion of grain boundaries, which increases the conductivity of the films obtained. Moreover, the increase of grain size could be attributed to the improvement of the crystallinity, which is confirmed by X-ray diffraction (XRD) and SEM micrograph. As a result, the quality factor of the film increases with increasing grain size. The lowest resistivity ($\rho = 0.53$ Ω cm) and maximum value of Hall mobility ($\mu = 1.51$ cm^2/Vs) are obtained for the thin layers deposited at 40 min. These values suggest that CuInGaS$_2$ thin film is a promising material for photovoltaic applications. Similar carrier concentration, resistivity, conductivity and mobility values are reported for CuInS$_2$ films prepared by magnetron sputtering [50], Cu$_2$SnS$_3$ films prepared by co-evaporation [51] and Cu$_2$ZnSnS$_4$ thin films absorbers by electro-deposition [52].

4 Conclusion

In brief, the studies reported here show that it is possible to deposit CuInGaS$_2$ films using spray pyrolysis technique in ambient atmosphere using compressed air as carrier gas. The thin films were investigated using a variety of

Table 3 Electrical properties of thin films obtained at different deposition times

Name	Time (min)	Carrier concentration (1/cm^3)	ρ (Ωcm)	σ (1/Ωcm)	μ (cm^2/V s)	Type
HK-A1	25	1.3648E+19	2.5634E −1	3.9009E+0	1.7841E +0	p
HK-A2	30	1.5589E+18	5.6006E −1	1.7855E+0	7.1491E+0	p
HK-A3	40	7.7409E+18	5.3390E −1	1.8730E+0	1.5103E+0	p

characterization techniques including X-ray diffraction (XRD) with CuK ($\lambda = 0.154$ nm) radiation. XRD data used to calculate the grain size, the dislocation density and the lattice strain of the spray pyrolyzed CuInGaS$_2$ thin films. Raman scattering measurements have been performed on all samples. The Raman shifts near 240, 295 and 340 cm^{-1} are presumably belonging to E^3_{TO}, A^1_{LO} and E^1_{LO} modes of the CH-ordering of chalcopyrite phase. The surface morphology of CuInGaS$_2$ thin films was examined using scanning electron microscopy (SEM). The optical absorption spectra of CuInGaS$_2$ thin films have been recorded in the wavelength range 500–900 nm. Also, the optical band gap (E_g) (direct allowed transition), and width of the tail of the localized states were determined using the absorption spectrum fitting method (ASF). This method does not require the film thickness. In addition, the values of band gap (E_g) decrease from 1.54 to 1.50 eV by increasing the deposition time. For all samples band gap of the CuInGaS$_2$ thin films deposited at 375 °C was around 1.50 eV, which is very proper for solar conversion. The carrier concentration, mobility, resistivity and conductivity for the films deposited at 40 min are 7.74×10^{18} cm^{-3}, 1.51 cm^2/Vs, 5.34×10^{-1} Ω cm and 1.87 Ω^{-1}cm^{-1} respectively. By considering the values found for the electrical properties, we suggest that the time of 40 min is the good choice for the fabrication of CuInGaS$_2$ based solar cells. Structural, optical and electrical properties of sprayed films depend on the fabrication conditions, in particular on the time of spray.

References

1. W. Yao, Y. Wang, X. Wang, J. Zhu, Z. Zhang, X. Yuan, CuInS$_2$ thin films obtained by solid-state sulfurization. Mater. Sci. Semicond. Process. **26**, 175–181 (2014)
2. T. Watanabe, M. Matsui, Solar cells based on cuInS$_2$ thin films through sulfurization of precursors prepared by reactive sputtering with H$_2$S gas. Jpn. J. Appl. Phys. **35**, 1681–1684 (1996)
3. R. Scheer, I. Luck, M. Kanis, M. Matsui, T. Watanabe, T. Yamamoto, Incorporation of the doping elements Sn, N, and P in CuInS$_2$ thin films prepared by co-evaporation. Thin Solid Films **392**, 1–10 (2001)
4. M. Krunks, V. Mikli, O. Bijakina, H. Rebane, A. Mere, T. Varema, E. Mellikov, Composition and structure of CuInS$_2$ films prepared by spray pyrolysis. Thin Solid Films **361–362**, 61–64 (2000)
5. I. Oja, M. Nanu, A. Katerski, M. Krunks, A. Mere, J. Raudoja, A. Goossens, Crystal quality studies of CuInS$_2$ films prepared by spray pyrolysis. Thin Solid Films **480–481**, 82–86 (2005)
6. S. Kuranouchi, T. Nakazawa, Study of one-step electrodeposition condition for preparation of CuIn(Se, S)$_2$ thin films. Sol. Energy Mater. Sol. Cells **50**, 31–36 (1998)
7. M. Rafi, Y. Arba, B. Hartiti, A. Ridah, P. Thevenin, Optimization of growth of ternary CuInS$_2$ by spray pyrolysis for photovoltaic application. MJ Condens. Matter **14**, 31–35 (2012)
8. D. Souri, K. Shomalian, Band gap determination by absorption spectrum fitting method (ASF) and structural properties of different compositions of (60-x) V$_2$O$_5$-40TeO$_2$-xSb$_2$O$_3$ glasses. J. Non-Cryst. Solids **335**, 1597–1601 (2009)
9. L.E. Alarcon, A. Arrieta, E. Camps, S. Muhl, S. Rudil, E.V. Santiago, An alternative procedure for the determination of the optical band gap and thickness of amorphous carbon nitride thin films. Appl. Surf. Sci. **254**, 412–415 (2007)
10. M. Ajili, M. Castagn, N.K. Turki, Characteristics of CuIn$_{1-x}$Ga$_x$S$_2$ thin films synthesized by chemical spray pyrolysis. J. Lumin. **150**, 1–7 (2014)
11. A. Kotbi, B. Hartiti, A. Ridah, P. Thevenin, Characteristics of CuInS$_2$ thin films synthesizes by chemical spray pyrolysis. Optical Quantum Electron. **48**, 1–9 (2016)
12. T. Logu, K. Sankarasubramanian, P. Soundarrajan, J. Archana, Y. Hayakawa, K. Sethuraman, Vanadium doping induces surface morphological changes of CuInS$_2$ thin films deposited by chemical spray pyrolysis. J. Anal. Appl. Pyrolysis **122**, 230–240 (2016)
13. Technisch Physische Dienst, Delft, The Netherlands. (1975)
14. D. Lee, S. Park, J.H. Kim, Structural analysis of CIGS film prepared by chemical spray deposition. Curr. Appl. Phys. **11**(1), S88–S92 (2011)
15. C. Suryanarayana, M. Grant Norton, X-ray diffraction: a practical approach. (Springer, New York, 1998)
16. F.A. Akgul, G. Akgul, N. Yildirim, H.E. Unalan, R. Turan, Influence of thermal annealing on microstructural, morphological, optical properties and surface electronic structure of copper oxide thin films. Mater. Chem. Phys. **147**, 987–995 (2014)
17. B. Venugopal, B. Nandan, A. Ayyachamy, V. Balaji, Sankarakumar Amirthapandian, B.K. Panigrahi, B.K. Panigrahi, T. Paramasivam, Influence of manganese ions in the band gap of tin oxide nanoparticles: structure, microstructure and optical studies. RSC Adv. **4**, 6141–6150 (2014)
18. D.Y. Lee, J. Kim, Characterisation of sprayed CuInS$_2$ films by XRD and Raman spectroscopy measurements. Thin Solid Films **518**, 6537–6541 (2010)
19. S.B. Qadri, E.F. Skelton, D. Hsu, A.D. Dinsmore, J. Yang, H.F. Gray, B.R. Ratna, Size-induced transition-temperature reduction in nanoparticles of ZnS. Phys. Rev. B **60**(13), 9191–9193 (1999)
20. Yoan Bourlier, O.C. Robbe, C. Lethien, P. Roussel, A. Pastre, M. Zegaoui, N. Rolland, M. Bouazaoui, R. Bernard, Control of gallium incorporation in sol-gel derived CuIn$_{(1-x)}$Ga$_x$S$_2$ thin films for photovoltaic applications. Mater. Res. Bull. **70**, 137–144 (2015)
21. L. Bhir, T.B. Nasrallah, J.C. Bernede, S. Belgacem, Structural and optical properties of sprayed In$_{2-2x}$Al$_{2x}$S$_{3-3y}$O$_{3y}$ alloys. Mater. Chem. Phys. **72**, 320–325 (2001)
22. C. Gao, H. Shen, L. Sun, Z. Shen, Applied Surface Science **257**, 7529–7533 (2011)
23. Nader Ghobadi, Band gap determination using absorption spectrum fitting procedure. Int. Nano Lett. **3**, 2 (2013)
24. N.F. Mott, E.A. Davis, *Electron Process Non-Cryst. Mater* (Clarendon, Oxford, 1979)
25. J. Tauc, A. Menth, States in the gap. J. Non-Cryst. Solids **8–10**, 569–585 (1972)
26. D. Souri, M. Mohammadi, H. Zaliani, Effect of antimony on the optical and physical properties of Sb-V$_2$O$_5$-TeO$_2$ glasses. Electron. Mater. Lett. **10**, 1103–1108 (2014)

27. M. Pal, K. Hirota, Y. Tsujigami, H. Sakata, Structural and electrical properties of MoO$_3$-TeO$_2$ glasses. J. Phys. D: Appl. Phys. **34**, 459–464 (2001)

28. N. Chopra, A. Mansingh, G.K. Chadha, Electrical, optical and structural properties of amorphous V$_2$O$_5$-TeO$_2$ blown films. J. Non-Cryst. Solids **126**, 194–201 (1990)

29. D. Souri, S.A. Salehizadeh, Effect of NiO content on the optical band gap, refractive index, and density of TeO$_2$-V$_2$O$_5$-NiO glasses. J. Mater. Sci **44**, 5800–5805 (2009)

30. E. Johnson, R. K. Willardardson, A.C. Beer Eds; Academic Press, New York 157 (1967)

31. J. Tauc, A. Menth, States in the gap. J. Non-Cryst. Solids **8–10**, 569–585 (1972)

32. E. Aydin, M. Sankir, N.D. Sankir, Conventional and rapid thermal annealing of spray pyrolyzed copper indium gallium sulfide thin films. J. Alloys Compd. **615**, 461–468 (2014)

33. A.B.M. Shall, S. Jalal, A.H. Ahmed, M. Bhuiyan, Ibrahim, UV-Vis absorption spectroscopic studies of plasma-polymerized m-xylene thin films. Thin Solid Films **288**, 108–111 (1996)

34. M. Farahmandjou, S.A. Salehizadeh, The optical band gap and the tailing states determination in glasses of TeO$_2$-V$_2$O$_5$-K$_2$O system. Glass Phys. Chem. **39**, 473–479 (2013)

35. J. L. Shay, B. Tell, H. M. Kasper, L. M. Schiavone,p-d Hybridization of the Valence Bands of I-III-Vl$_2$ Compounds, physical review 5, 5003-5005 (1972)

36. A.S. Hassanien, Effect of Se addition on optical and electrical properties of chalcogenide CdSSe thin films. Superlattices Microstruct. **89**, 153–169 (2016)

37. S. Sindu, S. Sanghi, A. Agarwal, V.P. Seth, N. Kishore, Effect of Bi$_2$O$_3$ content on the optical band gap, density and electrical conductivity of MO·Bi$_2$O$_3$·B$_2$O$_3$ (M = Ba, Sr) glasses. Mater. Chem. Phys. **90**, 83–89 (2005)

38. A.S. Hassanien, A.A. Akl, Influence of composition on optical and dispersion parameters of thermally evaporated non-crystalline Cd$_{50}$S$_{50-x}$Se$_x$ thin films. J. Alloys Compd. **648**, 280–290 (2015)

39. S.A. Fayek, M. El-Ocker, A.S. Hassanien, Optical and electrical properties of Ge$_{10+x}$Se$_{40}$Te$_{50x}$ thin film. Mater. Chem. Phys. **70**(2), 231–235 (2001)

40. C.M. Muiva, T.S. Sathiaraj, J.M. Mwabora, Chemical bond approach to optical properties of some flash evaporated Se$_{100X}$Sb$_X$ chalcogenide alloys. Eur. Phys. J. Appl. Phys. **59**, 10301 (2012)

41. K. Hattori, K. Akamatsu, N. Kamegashira, J. Appl. Phys. **71**, 3414–3418 (1992)

42. Lin-Ya. Yeh, Kong-Wei Cheng, Growth and characterization of CuInS$_2$ nanoparticles prepared using sonochemical synthesis. J. Taiwan Inst. Chem. Eng. **48**, 87–94 (2015)

43. Ahmed Kotbi, Bouchaib Hartiti, Salah Fadili, Abderraouf Ridah, Philippe Thevenin, Copper indium gallium disulphide (CuInGaS$_2$) thin films deposited by spray pyrolysis for solar cells: influence of deposition time in controlling properties of sprayed CuInGaS$_2$ absorbers. Opt. Quant. Electron **48**(524), 1–13 (2016)

44. S. Bandyopadhyaya, S. Chaudhuri, A.K. Pal, Solar Energy Materials & Solar Cells **60**, 323–339 (2000)

45. A. Antony, A.S. Asha, R. Yoosuf, R. Manoj, M.K. Jayaraj, Growth of CuInS$_2$ thin films by sulphurisation of Cu–In alloys. Sol. Energy Mater. Sol. Cells **81**, 407–417 (2004)

46. S. Bandyopadhyaya, S. Chaudhuri, A.K. Pal, Synthesis of CuInS$_2$ films by sulphurization of Cu/In stacked elemental layers. Sol. Energy Mater. Sol. Cells **60**, 323–339 (2000)

47. L. Zhang, Q. He, W.L. Jiang, F.F. Liu, C.J. Li, Y. Sun, Solar Energy Materials and Solar Cells **93**, 114 (2009)

48. Y.H. Jo, B.C. Mohanty, Y.S. Cho, Solar Energy **84**, 2213–2218 (2010)

49. Z. Mustafa, Influence of grain size on electrical and optical properties of InP films. Chin. Phys. Lett. **25**(11), 4090–4092 (2008)

50. W. Ligang, W. Yanlai, Y. Wei, Z. Jun, X. Jingang, Effect of sulfurization time on the formation of CuInS2 thin films. Rare Metal Mater. Eng. **44**(4), 0805–0807 (2015)

51. T.S. Reddy, R. Amiruddin, M.C. Santhosh Kumar, Deposition and characterization of Cu2SnS3 thin films by co-evaporation for photovoltaic application. Solar Energy Mater. Solar Cells **143**, 128–134 (2015)

52. A. Tang, J. Liu, J. Ji, M. Dou, Z. Li, F. Wang, One-step electrodeposition for targeted off-stoichiometry Cu 2 ZnSnS 4 thin films. Appl. Surf. Sci. **383**, 253–260 (2016)